Glass Transition in Dendrimers

K. Karatasos

Chemical Engineering Department, Physical Chemistry Lab, Aristotle University of Thessaloniki, 54124 Thessaloniki, Greece

Received March 11, 2006; Revised Manuscript Received April 27, 2006

ABSTRACT: Molecular dynamics simulations were employed in order to examine the effects of the dendritic topology to the characteristics of local environment and its association with the manifestation of glass transition phenomena. Dendrimer models of the AB_2 type of generations 3, 4, and 5 were simulated in the melt state in a wide temperature range. Investigation of intradendrimer motional properties revealed that connectivity constraints inherent to this topology impose a strong dynamic contrast within the dendritic structure which increases with molecular size. This strong separation of the relevant time scales particularly at the largest size model, combined with structural rearrangements both of intra- and intermolecular nature, offers a new basis for the rationalization of recent experimental findings where existence of multiple dendrimer glass transitions was observed.

I. Introduction

Glass transition phenomena in soft condensed matter systems are intimately related to the details of local organization and dynamic rearrangement of the relevant glass-forming units.[1] Structural and/or motional frustration,[2] ergodicity breaking,[3] and dynamic heterogeneity[4] are among the commonly reported attributes for a variety of different systems near vitrification. Changes in thermodynamic variables,[5] specific interactions,[6] and topological features[7,8] are known to influence the manifestation and the properties of the approached glass state.

Particularly in polymers, connectivity enhances correlation of motion and promotes the cooperative nature of local relaxation. Additional factors like the existence of physical or chemical networks,[9,10] confinement, and interactions with surfaces[11−13] were found to be responsible for the modification of the characteristic time scale of polymer segmental motion (usually expressed in terms of the so-called α-relaxation), which drives the system to the glass state. When approaching glass transition (T_g) strong spatial heterogeneities are formed,[14] resulting in an enhanced dynamic contrast between different subregions. In special cases, e.g. when local motional mechanisms become activated in distinct microscopic arrangements or specific thermodynamic states, multiple glasslike transitions can be observed.[15−17]

Molecules bearing the dendritic morphology appear as ideal candidates for an investigation of the effects that strong connectivity constraints may impart on the mechanisms involved in the manifestation of polymer glass-transition phenomena. Their highly branched but regular structure can be described in a systematic manner. For constant total number of monomers and number of bonds between branching points, dendritic structure starting from a single-atom core corresponds to the minimum of the topological Wiener index,[18] representing thus the most compact object. Experimental findings like the existence of significant dynamic heterogeneities between monomers within the structure[19] or even indications for multiple glasslike transitions in dendritic materials[20] have already been reported. Details, however, on the underlying mechanisms responsible for this behavior still remain to be clarified.

In this work we have examined by means of molecular dynamics (MD) computer simulations a series of AB_2 dendrimers in the melt, exploring the role of the dendritic topology in the development of structural and motional heterogeneities as the systems approach the glassy state. Since the models used (see next section) were not in an atomistic representation that would correspond to specific dendrimers, no attempt is made for a quantitative comparison to actual dendritic molecules. Instead, our effort is focused on the description of the mechanisms involved in the manifestation of glass transition phenomena in the model systems examined, which however are expected to be comparable in a qualitative sense to the behavior of actual systems bearing the examined topology.

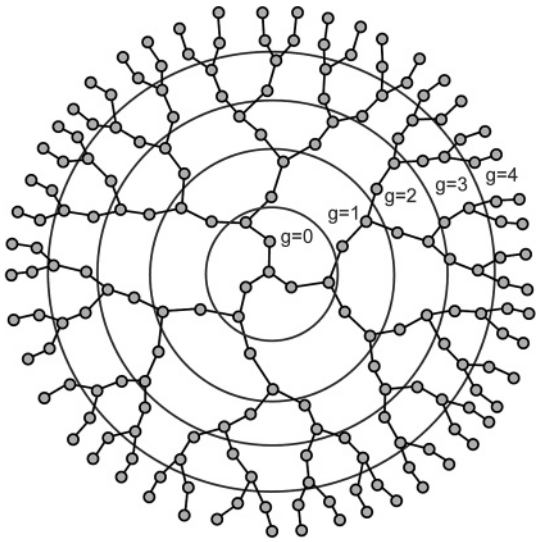

Figure 1. Schematic representation of a dendrimer model of the fourth generation (G4). The concentric circles indicate the boundaries of the different generational shells (g-shells).

II. Model Description

Molecular dynamics simulations in the constant temperature−constant pressure ($p = 1$ atm) ensemble were performed in the melt state utilizing the DLPOLY package,[21] in three united atom (UA) dendrimer models of different sizes with a topology schematically illustrated in Figure 1. The structure starts from

10.1021/ma060545z CCC: $33.50 © 2006 American Chemical Society
Published on Web 05/26/2006

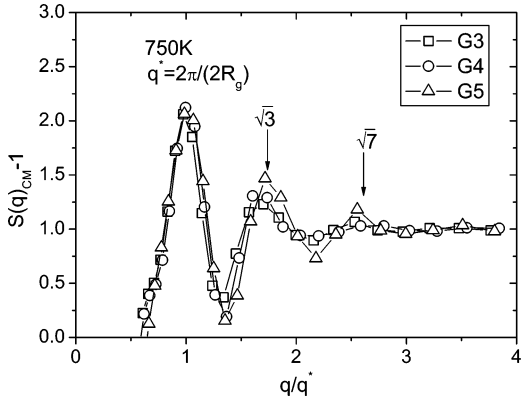

Figure 2. Static structure factor of the centers of mass for the examined systems at 750 K. Abscissa is scaled with a q value corresponding to the nominal interdendrimer separation $\simeq 2R_g$. Values for the radii of gyration at 750 K used for the scaling are $R_g(G3) = 6.1$ Å, $R_g(G4) = 7.7$ Å, and $R_g(G5) = 9.8$ Å. Arrows indicate locations of the peaks expected for a liquidlike structure.[35]

a trifunctional core and grows radially outward with every other bead branched (functionality 3) until the target generational shell is reached. The maximum generational shell g (starting from 0) denotes the generation G of the dendrimer. According to this scheme, molecules of generation 3, 4, and 5 consist of 91, 187, and 379 beads, respectively. The systems were simulated in a broad temperature range (300 K up to 800 K every 50 K) in the melt, comprised by 30 molecules for G3 and G4 systems and 25 molecules for G5. The simulation protocol (generation of initial structures, simulation force field, other simulation parameters, i.e., time step, potential cutoffs, procedure for equilibration and generation of production runs, etc.) used for G3 and G4 models (described in detail elsewhere[22]) was followed for the G5 systems as well. The only difference with respect to the smaller size systems was that G5 models were equilibrated for at least twice as long a period, while longer trajectories (up to 30 ns length) were generated in order to accomplish a satisfactory degree of decorrelation of local reorientational motion.

III. Static Properties/Local Structure

As was illustrated in our previous work,[22] small generation dendrimers in the melt are arranged in a liquidlike manner, assuming intermolecular distances essentially controlled by their size. Figure 2 includes the G5 model in the same picture. The static structure factor for the centers of mass (CM) of the dendrimers was calculated directly in the inverse space following the expression

$$S(q)_{CM} = 1 + \frac{1}{N}\left\langle \sum_{i=1}^{N}\sum_{j\neq i}^{N} \frac{\sin(qr_{ij})}{qr_{ij}} \right\rangle \qquad (1)$$

where q represents the magnitude of the scattering vector. Indices i, j refer to different molecules, while N is the number of molecules in each system. Angular brackets denote both time and ensemble average. $S(q)_{CM}$ is plotted in Figure 2 as a function of the magnitude of the scattering vector (each center of mass is considered as a scatterer), scaled by the value q^* which corresponds to the nominal interdendrimer distance ($\simeq 2R_g$). Such a scaling enables identification of the characteristic length scales associated with the dendrimers' arrangement in the bulk. The relative separation between the peaks appears compatible to a liquidlike arrangement[35] as pointed out by the arrows. A similar picture describes the lower temperatures as well.

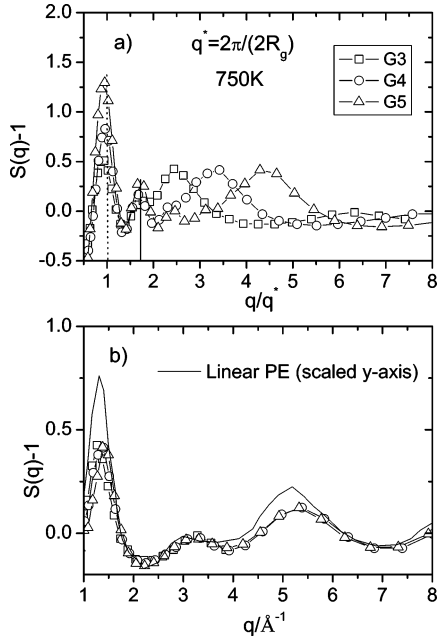

Figure 3. (a) Comparison of static structure factor of the examined systems at the same temperature. X-axis is scaled by a q value corresponding approximately to the interdendrimer distance $\simeq 2R_g$. Values of the radii of gyration used for the scaling are the same as in Figure 2. Vertical lines mark the peak positions appearing at the low-q regime. (b) Comparison of the dendrimer structure factors with the one describing an actual linear polyethylene model ($T = 430$ K) at the high-q regime. Y-axis values for the linear model have been scaled to facilitate comparison with the static structure factor from the dendrimers.

To check the arrangement of individual beads in the melt, we have calculated the static structure factor according to the expression

$$S(q) = 1 + \frac{N}{V}\int [g(r) - 1]\frac{\sin(qr)}{qr} 4\pi r^2 \, dr \qquad (2)$$

N here is the total number of scatterers (beads) inside the volume of the system, V is the average volume, and $g(r)$ denotes the radial distribution function (RDF). Figure 3a compares the static structure factor of the examined systems at 750 K. Evidently, locations of the peaks at the low q regime scale with the dendrimers' size, indicating two characteristic distances for long-range order: the average separation between the centers of mass of the molecules and a length scale comparable to the radius of gyration. At higher values of the scaled scattering vector, failure of the superposition prompts to the dendrimer-size-independent nature of the subsequent peaks. Figure 3b shows the analogous comparison with the abscissa unscaled, at a q-regime starting from a magnitude close to the onset of the previous failure of scaling. The experimentally measured static structure factor for a linear polyethylene (PE) analogue ($\rho \simeq 0.78$ g/cm^3, $M_w \approx 90\,000$)[23] is shown for reference purposes as well. The maxima at $q \simeq 1.4$ Å^{-1} correspond to the peaks deviating from the superposition at $q/q^* > 2$ in Figure 3a. Close agreement of the peak positions for scattering vector magnitudes larger than $q \simeq 1$ Å^{-1} (describing distances shorter than $\simeq 6$ Å) shows that local bead arrangement at such short distances is insensitive to dendrimer molecular weight and shares common features with the linear polymer behavior.

On the basis of this similarity in short length scales, we can draw useful analogies concerning local conformations of dendrimer structural units in their own microenvironment. Figure 4 compares the radial distribution functions describing a

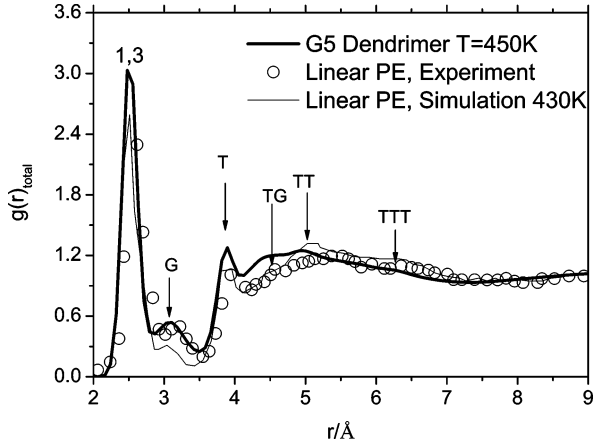

Figure 4. Comparison of RDFs (lines) describing a dendrimer model (G5, present work) and a linear UA polyethylene model (simulation, ref 24). Points correspond to data extracted from an experimental study in a linear PE sample. Arrows mark distances characteristic of distinct intramolecular conformations or conformational sequences.[24] Labels "G" and "T" denote the gauche and trans conformations, respectively. Label "1,3" indicates the distance between the first and the third united atom that form a bending angle.

dendimer model of the fifth generation, a UA PE model, and an actual linear PE system from an experimental study (see ref 24 and references therein). Labels "G" and "T" correspond to gauche and trans conformations, respectively. Assignment of characteristic distances to distinct conformations or conformational sequences follows ref 24. Apparently, all conformational peaks found in linear PE models characterize the dendrimer $g(r)$ as well. On the basis of this "mapping", we can monitor the relative changes of the labeled conformational states triggered by temperature variations. To distinguish between contributions of intra- or intermolecular origin, we have separately calculated the parts arising from intra- or intermolecular bead pairs. Figure 5 depicts the behavior of the distinct RDF contributions, at two temperatures 300 deg apart, for the largest (G5) and the smallest (G3) size models.

Comparing the responses of total $g(r)$ (upper panels) to temperature changes, we note similar trends between the two models. The intensity of all the conformational states appears increased at lower temperatures, implying an enhancement of local conformational heterogeneity. The depth of the minimum at ~3.5 Å increases at the lower temperature, while a clear tendency for separation between the "TG" and the "TT" peaks appears. To assess the origins of the observed changes, we resort to the examination of the separate intra- and intermolecular contributions. Since the intermolecular part remains 0 until ~3.5 Å, all the observed variations up to that distance arise from intradendrimer structural rearrangements. At longer distances though, local conformational changes appear as a combined effect of intra- and intermolecular contributions. It worths noticing that the intermolecular part of the RDF in the G3 model apart from exhibiting higher values also undergoes a larger relative change with temperature compared to the one in the G5 model. The explanation for this effect lies to the fact that the degree of dendrimer interpenetration (and thus the relative percentage of the intermolecular pairs) is significantly lower at the G5 model with respect to the one observed in smaller size dendrimers. To demonstrate this effect, we have calculated the average number of beads belonging to neighboring molecules that interpenetrate each dendrimer per unit volume (see ref 22 for more details). As shown in Figure 6, while for G3 and G4 models the number of interpenetrating beads assumes similar values and an almost indistinguishable temperature dependence, in the G5 system this number is on average more than 2 times lower and exhibits a weaker temperature dependence. These findings indicate that G5 dendrimer assumes a more compact structure compared to the lower generation dendrimers, which impedes interpenetration from neighboring dendrimer beads.

To quantify the development of local structural heterogeneity at length scales representative of rearrangements of intramolecular bead pairs, we can define an appropriate "conformational contrast" probe and follow its temperature dependence. Selection of such a probe was motivated from an earlier proposed method which aimed at the identification of a "microstructural signature" of glass transition and was successfully applied in Lennard-Jones liquids.[25] According to this method, the temperature dependence of the quantity $R = g_{min}/g_{max}$, defined as the ratio of the value of $g(r)$ at the first minimum (g_{min}) over its value at its first maximum (g_{max}), was found to change slope at the nominal glass transition. Since we are interested in changes of intramolecular origin, we consider the ratio $R = g_{min}/g_{max}$, where g_{max} corresponds to the "1,3" maximum of $g(r)$ (attributed to the distance between the first and the third united atom that form a bending angle) at $r \simeq 2.5$ Å (see Figure 5) and g_{min} the value of $g(r)$ at the minimum just before the "T" peak at $r \simeq 3.5$ Å (see inset in Figure 7) which practically coincides with the maximum distance at which intermolecular contributions remain negligible. Application of this method resulted in the temperature dependence of R as depicted in Figure 7. A single change in the slope of R is detected at the lower generation systems (G3, G4), at temperatures very close to the respective glass transitions (T_g(G3) $\simeq$ 500 K, T_g(G4) $\simeq$ 550 K),[22] lending credence to the utilization of this method for the detection of microstructural changes close to T_g. On the other hand, data for the G5 system are better described if three different temperature regimes are assumed, implying the existence of two nominal transitions.

The consideration of three temperature regimes is based on a simple linear regression analysis which involves a succession of steps in the fitting procedure. Starting from the three points corresponding to the higher temperatures, the correlation coefficient of the linear fit is calculated. At the following step, the point of the next temperature is included in the fit, and the new correlation coefficient is estimated. The same procedure continues on, to the point where the quality of the linear fit drops considerably. The set of points that maximized the correlation coefficient is considered to form the (first) straight line. The procedure is then repeated starting from the first point that was not included in the previous straight line, and the set of points comprising the next line is determined likewise. The three last points corresponding to the lower temperatures that were not found to belong in the first two lines are considered to belong in a single (third) straight line.

Another method commonly employed for identification of glasslike transitions is through the temperature dependence of the specific volume. In this case changes in the density of the entire system are probed, so that synergistic rearrangements of intermolecular nature certainly participate. Figure 8 plots the specific volume for systems G3 and G4 as calculated in our earlier work,[22] together with the one measured in the present study for the largest G5 system. Once more, an optimal description of G5 data in terms of the iterative fitting procedure described earlier prompts for two consecutive changes in the slope at temperatures compatible with the ones detected from the dependence of the R ratio (Figure 7). Therefore, similar nominal transition temperatures are identified, either by means of a conformational-based intramolecular criterion or via a

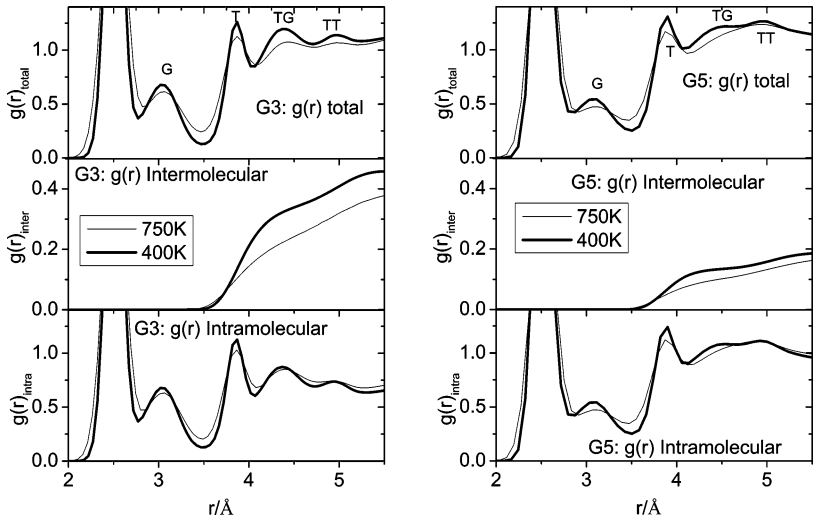

Figure 5. Comparison of intermolecular, intramolecular, and total RDFs for the smallest (left) and the largest (right) size dendrimers at 450 and 750 K. Upper panels: total $g(r)$. Middle panels: intermolecular part. Lower panels: intramolecular part. Conformational peaks are labeled after the linear PE model.

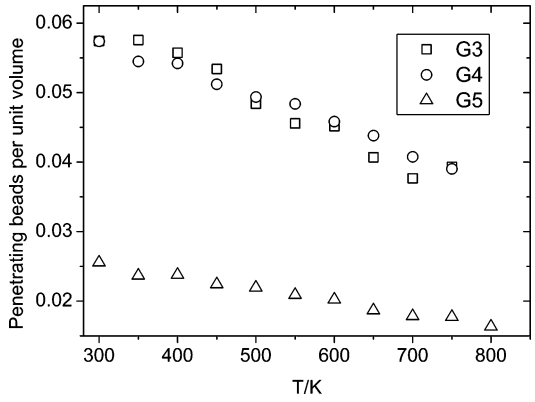

Figure 6. Temperature dependence of the average number of interpenetrating beads from neighboring molecules per unit volume, for all the models studied.

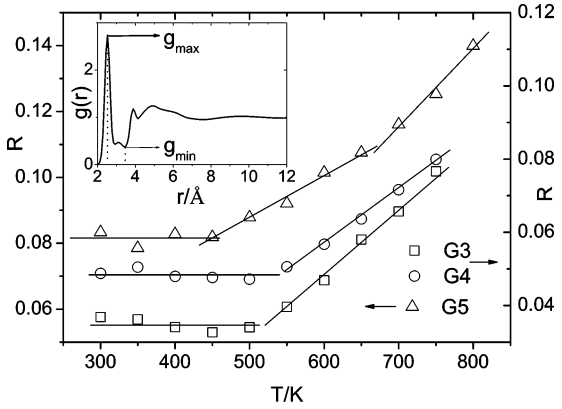

Figure 7. Temperature dependence of ratio R (see text) for the examined systems. Straight lines denote the slopes in different temperature regimes. Inset illustrates the definitions of g_{min} and g_{max} as described in the text.

system-wide probe involving intermolecular contributions as well.

IV. Dynamic Properties

A dynamic probe for the proximity of a system to the glassy state is the formation of strong motional heterogeneities in the local environment[14,26] which are accompanied by a significant increase of segmental relaxation times.[27] In this context, we have

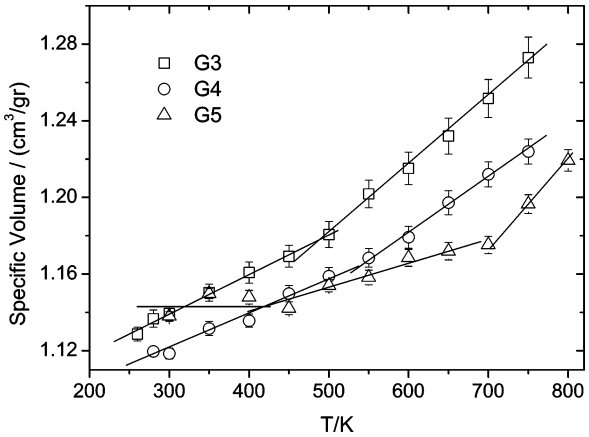

Figure 8. Temperature dependence of the specific volume for the systems studied. Straight lines denote the slopes in the different temperature regimes.

examined aspects of local motion and probed for the presence of dynamic heterogeneities between different subregions within the dendrimer interior.

A. Mean-Square Displacement: Mobility Contrast. From the study of the transition rates of torsional angles located at different generational shells within the G3 and G4 models,[22] it was noted that due to the less hindered motion, generational shells near the dendrimer periphery exhibited much higher mobility compared to the ones closer to the topological center. It was also shown that at temperatures near the nominal T_g the bulk of the average conformational activity was arising from contributions of the outer generations.

In Figure 9 the dynamic contrast between the two outer shells g_i and g_{i-1} is quantified by calculating the ratios of the mean-square displacements (MSD) $DR_{(i,i-1)} = \langle \Delta r_{g_i}^2 \rangle / \langle \Delta r_{g_{i-1}}^2 \rangle$ of the relevant beads for the lower (G3, $i = 3$) and the higher (G5, $i = 5$) generation models. For the G3 model, an abrupt decrease of the MSD ratio takes place in the vicinity of the apparent glasslike transition (≃500 K). A similar change occurs for the G5 model, near the region of the "high-temperature" nominal glasslike transition as can be inferred from the temperature dependence of the specific volume and the R ratio (Figures 7 and 8). A notable difference between the G3 and the G5 behavior, though, is that in the small size dendrimer the ratios below 500 K do not seem to undergo any significant change,

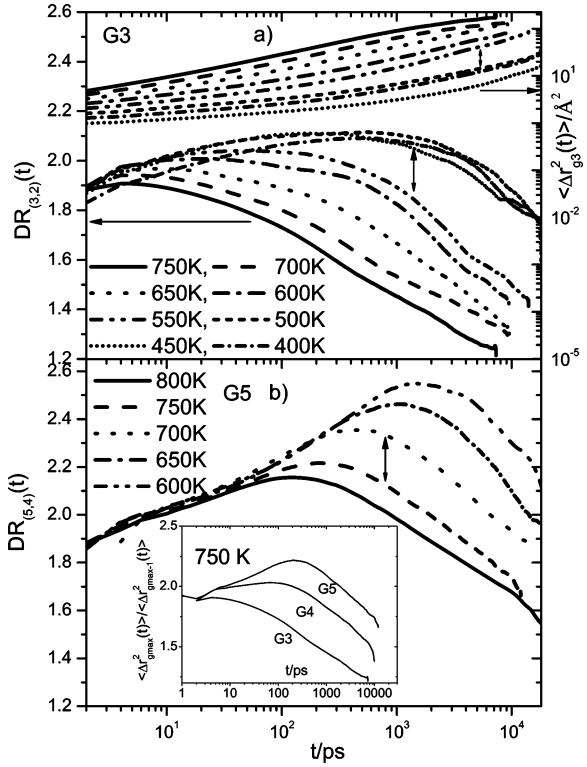

Figure 9. (a) Left scale: MSD ratio (see text) between the two outer generational shells for the G3 model at temperatures above and below the nominal T_g (≃500 K). Right scale: MSD of the beads belonging to the outer generational shell. Double arrows emphasize the sudden decrease occurring near the glasslike transition. (b) MSD ratios (see text) for the G5 dendrimers. The double arrow indicates the relative reduction of the ratio between temperatures above and below the "high temperature" nominal T_g. Inset displays the comparison of the mobility ratios at a constant temperature for the three examined systems.

while the ratios of the larger generation model assume increasingly higher values. At the same time the observed maxima shift to longer times. This augmentation of ratios for the G5 model continues until $T = 450$ K. At that point the tendency is reversed, until the maximum value of the ratios levels off to a magnitude of 2.0, in a fashion similar to the one observed in the G3 model. The inset of Figure 9b indicates that the values of the MSD ratios (shown here at a temperature above the nominal T_gs) are size-dependent, suggesting that a dynamic contrast develops between analogous shells upon generation (G) growth.

To gain a deeper insight into the apparent mobility difference between generational shells, it is helpful to attempt an interpretation for the peak-shaped temporal evolution of the mobility ratios. Examination of the time dependence of the associated MSD curves (not shown here) indicated that the initial rise of the mobility contrast is due to a lower increase rate of the MSD of the next-to-the-outer g-shell compared to that of the outer shell's. This tendency continues up to the characteristic time where the ratio assumes its maximum. The drop that follows is triggered by a sudden increase of the next-to-the-outer shell's MSD. Such behavior is compatible with a motional confinement/release process which presumably is activated with a time lag in beads belonging to different generational shells. A mechanism like that has already been described for a number of different systems and is related to the escape of the glass-forming units from a "cage" formed by their immediate neighbors.[28] The representative time scale for this escape mechanism (decaging) is usually placed at the crossover region between a subdiffusional and the diffusional regime characterizing α-relaxation.

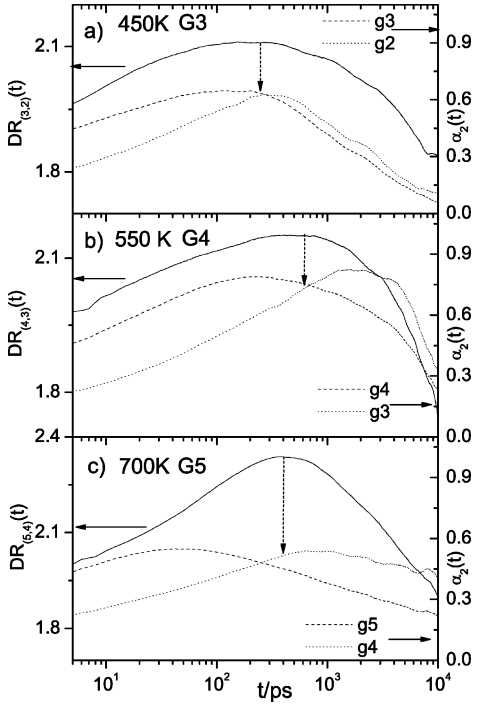

Figure 10. Left axes: MSD ratios $DR_{(i,i-1)}$ (see text). Right axes: non-Gaussian parameter for the two outer shells. Dashed and dotted curves correspond to the outer and to the next-to-the-outer generational shells, respectively. (a) G3 model, (b) G4 model, and (c) G5 model. Long short-dashed arrows indicate peak locations for the MSD ratios.

The time scale for the decaging has also been associated with the time occurrence t^* of the maximum of the non-Gaussian parameter,[4,29] defined as $\alpha_2(t) = {}^3/_5\langle[r(t) - r(0)]^4\rangle/\langle[r(t) - r(0)]^2\rangle^2 - 1$. This parameter is commonly employed for the quantification of the deviation of a particle's motion from the Gaussian behavior.[30] Following this argument we have calculated the non-Gaussian parameter at different temperatures for the two outer shells and compared the corresponding t^* to the time at which the mobility ratios exhibit maxima (Figure 10). For all generation models the MSD ratios peak at a time scale intermediate between the t^* of the non-Gaussian parameters describing the two neighboring g-shells. The same behavior was also observed at different temperature−distances from the nominal T_gs. The scenario emerging from this observation implies that the mobility contrast among different g-shells of the same dendrimer as well as its peak shape originates from the fact that the decaging processes at the neighboring g-shells occur at distinct time scales. The ratio increases since beads of the outer g-shell approach the escape-time while those belonging to the neighboring g-shell move slowly within the boundaries of their cage. It peaks at a time after the onset of decaging of the outer g-shell's beads and starts decreasing close to the time of the escape of the inner g-shell's beads from their cage.

B. Local Reorientational Motion. Bond reorientational motion is a local relaxational mechanism directly related to α-relaxation, which is associated with the length and the time scale of the cooperative rearrangements close to the glass transition.[27,32] This motion becomes experimentally accessible via the spin−lattice (T_1) relaxation time in nuclear magnetic resonance measurements.[14] The latter is calculated through the spectral density $J(\omega) = {}^1/_2\int_{-\infty}^{\infty} P_2(t)e^{i\omega t}\,dt$ which involves the second-order bond orientational correlation function $P_2(t) = {}^1/_2\langle 3[\hat{h}(t)\cdot\hat{h}(0)]^2 - 1\rangle$ ($\hat{h}$ symbolizes the unit vector along an examined bond).

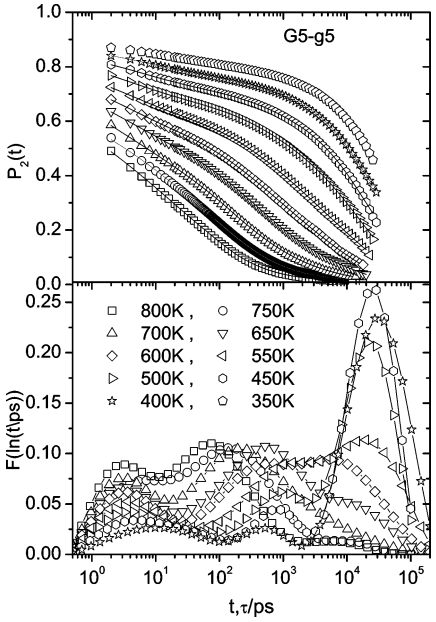

Figure 11. Upper panel: reorientational correlation functions for bonds belonging to the last generational shell (g5) of the G5 dendrimer in different temperatures. Lines through the points denote the fits resulted from the DRT analysis. Lower panel: corresponding DRTs.

As shown in our previous study,[22] this dynamic probe is sensitive to the proximity to the glassy state, tracking down the anticipated slowdown in local motion. To substantiate whether the mobility contrast observed within the dendrimer structure by means of bead displacements is reflected on the correlated bond reorientation as well, we have separately calculated $P_2(t)$ for bonds in different g-shells. Analysis of dynamic spectra was performed by calculation of the distribution of relaxation times (DRT).[33] In the context of this method, dynamic spectra are described as a continuous superposition of single-exponential processes with a distribution function $F(\ln \tau)$ which is normalized in the logarithmic scale. Motional mechanisms well separated in time scale appear as different peaks in the calculated distributions. In the case of almost symmetric peaks, a good estimation of the characteristic time (CT) for each process can be extracted from the time location of the corresponding maxima. An overall average relaxation time can be calculated by $\tau_{av} = \int_{-\infty}^{\infty} \tau F(\ln \tau)\, d \ln \tau$, which is equivalent to the time extracted by integration of the correlation function.

An example of calculated correlation functions together with the corresponding distributions are displayed for the outer g-shell of the G5 dendrimer in Figure 11. Analogous spectra for the G3 and the G4 systems have been described elsewhere.[22] Visual inspection of the correlation functions attests to the shift of their tails to longer times as the temperature decreases. On the basis of the spectral features of the distributions, one can divide them into two groups: those below 650 K and those above. In the "high temperature" group, the DRTs are characterized by two peaks: one due to an ultrafast process at the picosecond time scale exhibiting a virtually temperature-independent CT and one with a strongly temperature-dependent peak-position. The former can be ascribed to fast librational motions around the torsional energy minima,[32,34] while the latter is apparently responsible for the observed dynamic slowdown as the temperature decreases. At 650 K, the slow process appearing in the spectra of the first group splits into two maxima: an intermediate peak which remains present in all the distributions of the "low temperature" group and a slower process that gains amplitude and shifts to longer times upon temperature decrease. The temperature at which the intermediate process appears practically coincides with the "high temperature" nominal glass transition as detected from the dependence of the specific volume and from the R ratio in the G5 systems (section III). For comparison purposes, Figure 12 presents the temperature dependence of the DRTs corresponding to bond reorientational spectra describing outer g-shells for all the models. As pointed out in the relevant plots (short dashed arrows), the occurrence of an additional process is also noted in spectra corresponding to the nominal glass-transition temperatures in G3 and G4 models. Spectral features of the intermediate peak, like its relatively fast time scale, its weak temperature dependence (as inferred from its peak position), and its low amplitude, are compatible with a rather fast and localized motion.

A reasonable candidate for such a mechanism is the less-hindered motion of bonds close to the dendrimer periphery. This notion is corroborated by the fact that this peak assumes its higher amplitude for bonds belonging to the outer g-shell, while for g-shells closer to the dendrimer core (relevant DRTs are not shown here) its amplitude is rapidly reduced. This scenario implies that close proximity to the glass transition induces some kind of dynamic "microphase separation" between fast and slow relaxing bonds, its signature being the appearance of the intermediate peak. Since the percentage of bonds close to the periphery is significantly reduced due to the backfolding effect,[22] the amplitude of this peak is rather low. Moreover, because of the lower energy barrier that such a motion would need to overcome, the apparent temperature dependence of its characteristic time appears to be very weak. The slower process, therefore, could be attributed to relaxation of the majority of the bonds (hence the much higher amplitude) which "feel" the proximity to the glassy state in a more drastic manner, in the sense that complete loss of the orientational memory would involve the cooperative motion of neighboring beads and the reorientation of the entire dendrimer molecule (hence the slower time scale), which become increasingly difficult close to glass transition. An analogous dynamic process arising from "free" bond reorientation close to glass formation in linear polymers would be harder to detect due to the much lower amplitude that such a mode would possess (few bonds close to the chain ends would only participate). The significant increase of the slower mode's amplitude close to the nominal T_g is indicated in Figure 12 by double arrows. A similar augmentation of the slower peaks's amplitude takes place close to the "lower temperature" nominal glass transition for the G5 system, alluding to the existence of a "second level" freezing-in event in the large system.

On the basis of the above scenario, we can now rationalize the shift of the maxima of the MSD ratios to longer times with dendrimer size (inset in Figure 9b), as described in section IVA. Bonds closer to the surface may relax faster, while for bonds closer to the core the entire molecule reorientation plays a more important role. In low dendrimer sizes global rotation is a relatively fast process, keeping thus dynamic contrast among g-shells at low levels. As size grows global reorientation becomes significantly slower, creating a stronger dynamic contrast between g-shells, which can be manifested as an increasing time lag in their corresponding decaging processes.

Figure 13 portrays the temperature dependence of inverse average relaxation times extracted from spectra of different g-shells for the two extreme dendrimer sizes. It should be noted that due to the relevant amplitudes and the time scales of the processes (see Figure 12), the average times is influenced the most by the slower mode's behavior. Comparison of the relative

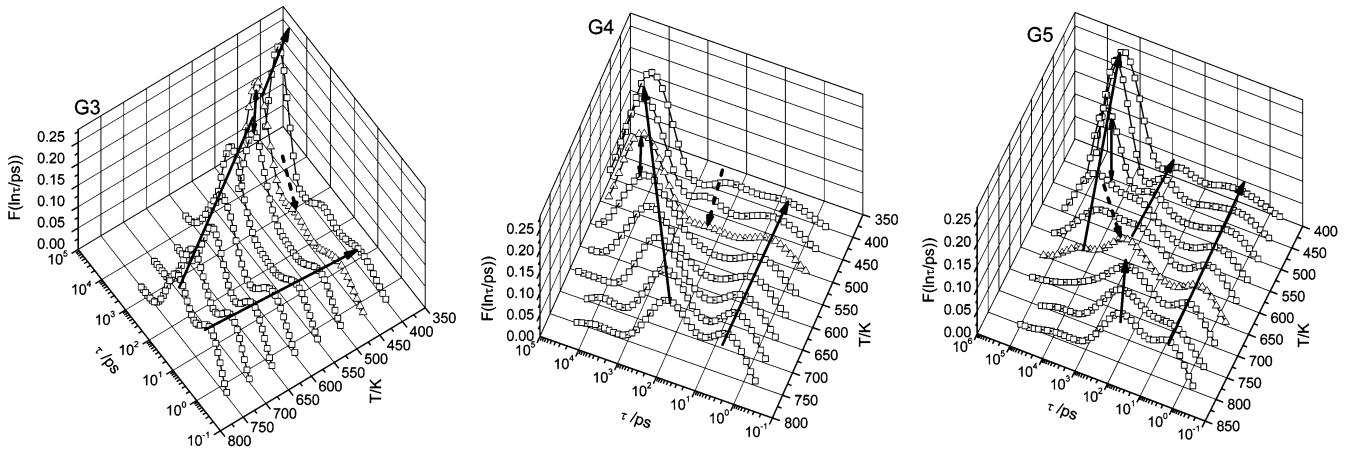

Figure 12. A 3-dimensional representation of the distributions corresponding to P_2 correlations functions for the outer g-shells. Distributions at which the intermediate process appears at first are drawn with a triangle symbol, and the peak position is marked by a dashed arrow. Long arrows follow the peak positions of the detected processes. Double arrows indicate the change in amplitude of the slow process (see text).

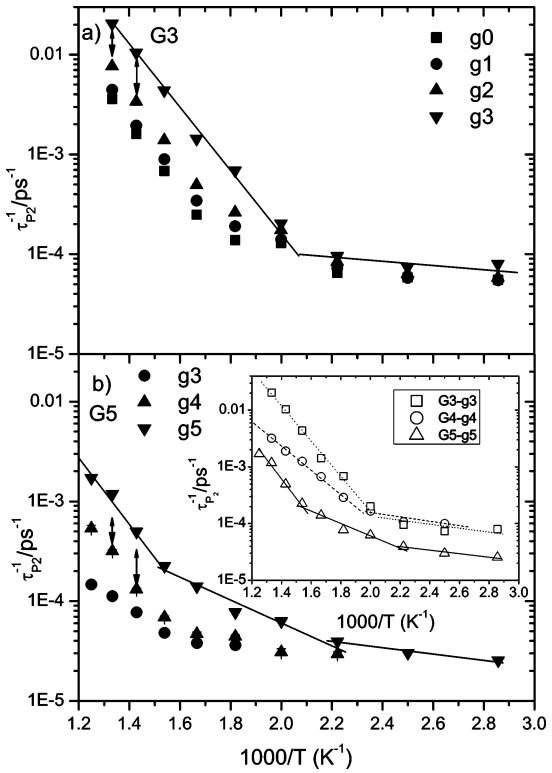

Figure 13. Inverse average P_2 bond relaxation times for different g-shells. Error bars are estimated to be of the order of the symbols' size. Lines denote the different slopes describing the data (see text). (a) G3 model and (b) G5 model. Double arrows denote the difference in relaxation rates between the two outer g-shells for the G3 model. The same arrows are translated at corresponding temperatures of the G5 system to show relative differences in relaxation rates between the two models. Inset depicts the temperature dependence of inverse relaxation times for the outer g-shells of the examined models.

behavior for times describing equidistant-from-the-outer g-shells reveals that in the higher generation dendrimer at temperatures above the transition the dynamic contrast is enhanced. The size of the double arrows appearing in Figure 13a denotes the differences in the logarithms (and thus the ratios in linear scale) of the relaxation rates describing the two outer g-shells of the G3 model. The *same* arrows are translated to the respective inverse temperatures of the two outer g-shells in the G5 model (Figure 13b). The distances in the larger size model have been increased compared to the smaller size one, by approximately 40% and 14% at temperatures 750 K and 700 K, respectively.

The change in slope in the G3 model (Figure 13a) apparently represents the dynamic signature of the glasslike transition which is in consensus with the one identified by the static properties (Figures 7 and 8). The same conclusion can be drawn for the G4 model as well. For the G5 system, application of the iterative linear regression analysis described in section III implies two consecutive changes in slope as schematically shown in Figure 13b. The characteristic slope-change temperatures are in close agreement with the ones which provide a better description of the specific volume and the *R* ratio data (Figures 7 and 8). Temperature dependencies of the times describing reorientational motion at the outer g-shell (which is comprised by more than half of the total number of bonds in each molecule) are collated in the inset of Figure 13b, where the effect of molecular size is clearly manifested.

V. Summary/Conclusions

In this work we have presented results from MD simulations of AB_2-type dendrimer melts, exploring the effects of topology and size in local structural and motional characteristics associated with the observation of glass-transition phenomena. Information arising from examination of static/conformational features shows that glassy behavior is sensitively reflected to intramolecular local packing characteristics as demonstrated by the *R* ratio behavior (Figure 7). Intermolecular factors enter through the dendrimer interpenetration (Figure 6) and affect mainly less localized conformations (Figures 4 and 5). The lower degree of interpenetration observed in the larger dendrimer, combined with the almost "in-phase " response of intramolecular (*R* ratio, Figure 7) and system-wide "glass probes" (specific volume, Figure 8) on temperature variation, implies that in large dendrimer systems changes in volumetric properties are mainly driven by intramolecular structural rearrangements.

As the size of the dendrimer grows, mobility contrast between different g-shells is progressively increasing (inset in Figure 10b, Figure 13). For constant dendrimer size, the time scales governing such bead rearrangements vary within the dendritic structure as evidenced by examining the MSD ratios (Figure 9) and the occurrence of distinct decaging times of beads belonging to different generational shells (Figure 10). Upon temperature decrease, a further enhancement of these dynamic heterogeneities may shift time scales for local motion sufficiently far apart for distinct freezing-in times to be realized (Figure 13). Whenever such a freezing-in event of local motion occurs, structural rearrangements are arrested and a glasslike transition is observed. Particularly for the beads belonging to the outer

g-shell, a number of which are located at the periphery while a part of them are backfolded toward the center of the structure, dynamic heterogeneity close to glass transition is manifested by the appearance of two motional processes (apart from the ultrafast librational mode) in the reorientational motion of bonds connecting them. The one characterized by the faster time which shows the weaker temperature dependence can be attributed to the relatively free motion of bonds close to the periphery. The slower mechanism represents bonds for which complete loss of orientational memory would involve cooperative rearrangements of neighboring beads as well as reorientation of the entire molecule, which are strongly temperature-dependent processes.

Although specific topological details of the dendritic structure (i.e., different spacer length between branching points or different branching functionality) may result in certain differentiations from the conclusions drawn here, it is believed that the results described in this work capture generic features of the dendrimer glass behavior. Future, more systematic experimental studies with sufficient spatial and temporal resolution (e.g., nuclear magnetic resonance studies or neutron scattering experiments) would certainly help toward the assessment of such issues.

Acknowledgment. Funding from the Greek General Secretariat for Research and Technology under the framework of the PENED 2003 program is gratefully acknowledged. Part of this work was carried out under the HPC-EUROPA project (RII3-CT-2003-506079), with the support of the European Community−Research Infrastructure Action under the FP6 "Structuring the European Research Area" Programme. The author thanks J. Baschnagel and A. V. Lyulin for helpful discussions.

References and Notes

(1) Debenedetti, P.; Stillinger, F. *Nature (London)* **2001**, *410,* 259.
(2) Vlassopoulos, D. *J. Polym. Sci., Polym. Phys.* **2004**, *42,* 2931.
(3) Puertas, A.; Fuchs, M.; Cates, M. *Phys. Rev. Lett.* **2002**, *88,* art. no. 098301.
(4) Kob, W.; Donati, C.; Plimpton, S. J.; Poole, P. H.; Glotzer, S. C. *Phys. Rev. Lett.* **1997**, *79,* 2827.
(5) Angell, C. *Proc. Natl. Acad. Sci. U.S.A.* **1995**, *92,* 6675.
(6) Rocher, N.; Frech, R. *Macromolecules* **2005**, *38,* 10561.
(7) Beiner, M.; Schroeter, K.; Hempel, E.; Reissig, S.; Donth, E. *Macromolecules* **1999**, *32,* 6278.
(8) Garcia-Domenech, R.; de Julian-Ortiz, J. *J. Phys. Chem. B* **2002**, *106,* 1501.
(9) Ryckaert, J.-P. *Comput. Phys. Commun.* **2005**, *169,* 89.
(10) Kalakkunnath, S.; Kalika, D.; Lin, H.; Freeman, B. *Macromolecules* **2005**, *38,* 9679.
(11) Anastasiadis, S.; Karatasos, K.; Vlachos, G.; Manias, E.; Giannelis, E. *Phys. Rev. Lett.* **2000**, *84,* 915.
(12) Smith, G.; Bedrov, D.; Borodin, O. *Phys. Rev. Lett.* **2003**, *90,* art. no. 226103.
(13) Serghei, A.; Kremer, F. *Phys. Rev. Lett.* **2003**, *91,* art. no. 165702.
(14) Ediger, M. *Annu. Rev. Phys. Chem.* **2000**, *51,* 99.
(15) Pham, K.; Puertas, A.; Bergenholtz, J.; Egelhaaf, S.; Moussaid, A.; Pusey, P.; Schofield, A.; Cates, M.; Fuchs, M.; Poon, W. *Science* **2002**, *296,* 104.
(16) Yildirim, Z.; Wuebbenhorst, M.; Mendes, E.; Picken, S.; Paraschiv, I.; Marcelis, A.; Zuilhof, H.; Sudhoeler, E. *J. Non-Cryst. Solids* **2005**, 2622.
(17) Vignaud, G.; Bardeau, J.; Gibaud, A.; Grohens, Y. *Langmuir* **2005**, *21,* 8601.
(18) Widmann, A.; Davies, G. *Comput. Theor. Polym. Sci.* **1998**, *8,* 191.
(19) Chai, M. H.; Niu, Y. H.; Youngs, W. J.; Rinaldi, P. L. *J. Am. Chem. Soc.* **2001**, *123,* 4670.
(20) Kruger, J. K.; Veith, M.; Elsasser, R.; Manglkammer, W.; Le Coutre, A.; Baller, J.; Henkel, M. *Ferroelectrics* **2001**, *259,* 27.
(21) Forester, T.; Smith, W. CCLRC, Daresbury Laboratory, Daresbury, Warrington Wa4 4AD, England. DL_POLY is a parallel molecular dynamics package developed at Daresbury laboratory, and is a property of the Council for the Central Laboratory of the Research Councils (CCLRC).
(22) Karatasos, K. *Macromolecules* **2005**, *38,* 4472.
(23) Honnell, K.; McCoy, J.; Curro, J.; Schweizer, K.; Narten, A.; Habenschuss, A. *J. Chem. Phys.* **1991**, *94,* 4659.
(24) Pant, P. V. K.; Han, J.; Smith, G. D.; Boyd, R. H. *J. Chem. Phys.* **1993**, *99,* 597.
(25) Wendt, H. R.; Abraham, F. F. *Phys. Rev. Lett.* **1978**, *41,* 1244.
(26) Caprion, D.; Matsui, J.; Schober, H. *Phys. Rev. Lett.* **2000**, *85,* 4293.
(27) Paul, W.; Smith, G. *Rep. Prog. Phys.* **2004**, *67,* 1117.
(28) Doliwa, B.; Heuer, A. *Phys. Rev. Lett.* **1998**, *80,* 4915.
(29) Baschnagel, J.; Varnik, F. *Condens. Matter* **2005**, *17,* R851.
(30) Arbe, A.; Colmenero, J.; Monkenbusch, M.; Richert, R.; Farago, B.; Frick, B. *Phys. Rev. Lett.* **2002**, *89,* art. no. 245701.
(31) Karatasos, K.; Adolf, D. B.; Davies, G. R. *J. Chem. Phys.* **2001**, *115,* 5310.
(32) Karatasos, K.; Ryckaert, J. *Macromolecules* **2001**, *34,* 7232.
(33) Provencher, S. A general-purpose constrained regularization method for inverting photon correlation data. In *Photon Correlation Techniques in Fluid Mechanics*; Schulz-DuBois, E. O., Ed.; Springer-Verlag: Berlin, 1983.
(34) Moe, N.; Ediger, M. *Macromolecules* **1995**, *28,* 2329.
(35) Guinier, A. *X-ray Diffraction;* Freeman & Co.: San Francisco, 1963.

MA060545Z